Heliyon 9 (2023) e16462

Contents lists available at ScienceDirect

Heliyon

journal homepage: www.cell.com/heliyon

Research article

Accelerated aging of unencapsulated flexible GaInP/GaAs/InGaAs solar cells by means of damp heat and thermal cycling tests

Xiaoxu Wu [a,b], Junhua Long [b,*], Qiangjian Sun [b], Xia Wang [b], Zhitao Chen [b], Menglu Yu [b], Xiaolong Luo [b], Xuefei Li [b], Huyin Zhao [b], Shulong Lu [b,**]

[a] School of Nano-Tech and Nano-Bionics, University of Science and Technology of China, Hefei, 230026, China
[b] Key Laboratory of Nanodevices and Applications, Suzhou Institute of Nano-Tech and Nano-Bionics, Chinese Academy of Sciences, Suzhou, 215123, China

ARTICLE INFO

Keywords:
Flexible III-V solar cells
GaAs solar cells
Damp heat
Thermal cycling
Recombination

ABSTRACT

The extended damp heat and thermal cycling tests were performed on unencapsulated flexible thin-film GaInP/GaAs/InGaAs solar cells to assess the long-term stability. The solar cells were subjected to 85 °C/85% damp heat test for more than 1000 h and 420 cycles of thermal cycling test between −60 °C and 75 °C, respectively. The performance attenuations of flexible solar cells were less than 2% in both cases, which were due to the slow decline of the open-circuit voltage with aging time. The slight decrease in open voltage was attributed to the increase in reverse saturation current due to the enhanced recombination, which was in good agreement with the calculation based on the two-diode model. The good performance of the unencapsulated flexible GaInP/GaAs/InGaAs solar cells in severe environment indicated the stable and reliable device fabrication art in the experiment.

1. Introduction

Flexible III-V thin-film solar cells provide a new application prospect for spacecraft that require a power supply, such as near space airships, drones, satellites, or space stations [1–4], due to the advantages of high efficiency [5], high flexibility, lightweight [6], and high radiation resistance [7]. In order to satisfy the long-term stable operation of solar cells, it is necessary to pay attention to the reliability. As well known, temperature and humidity are the two principal factors affecting the stability of solar cells in practical applications, which result in the degradation of photoelectric and material properties [8–11]. The flexible solar cells are exposed to complex environmental conditions in long-term operation. For example, they will be subjected to a wide range of temperature fluctuations in the alternation of day and night. Furthermore, strict requirements are placed on the anti-reflective coating (ARC) and metallization integrity of the solar cells in the adverse storage conditions with moisture and contaminants [12–15]. Therefore, it is of great significance to explore the long-term stability of flexible solar cells under damp heat and thermal cycling environment.

At present, the reliability analysis of III-V multi-junction solar cells mainly focuses on the degradation mechanism of unencapsulated rigid Ge and GaAs substrate solar cells under high-temperature thermal stress [16–19]. In addition, some studies have also mentioned the excellent stability of flexible glass-encapsulated multi-junction solar cells in aging experiments [20,21], but the

* Corresponding author.
** Corresponding author.
E-mail addresses: jhlong2017@sinano.ac.cn (J. Long), sllu2008@sinano.ac.cn (S. Lu).

https://doi.org/10.1016/j.heliyon.2023.e16462
Received 10 March 2023; Received in revised form 11 May 2023; Accepted 18 May 2023
Available online 19 May 2023

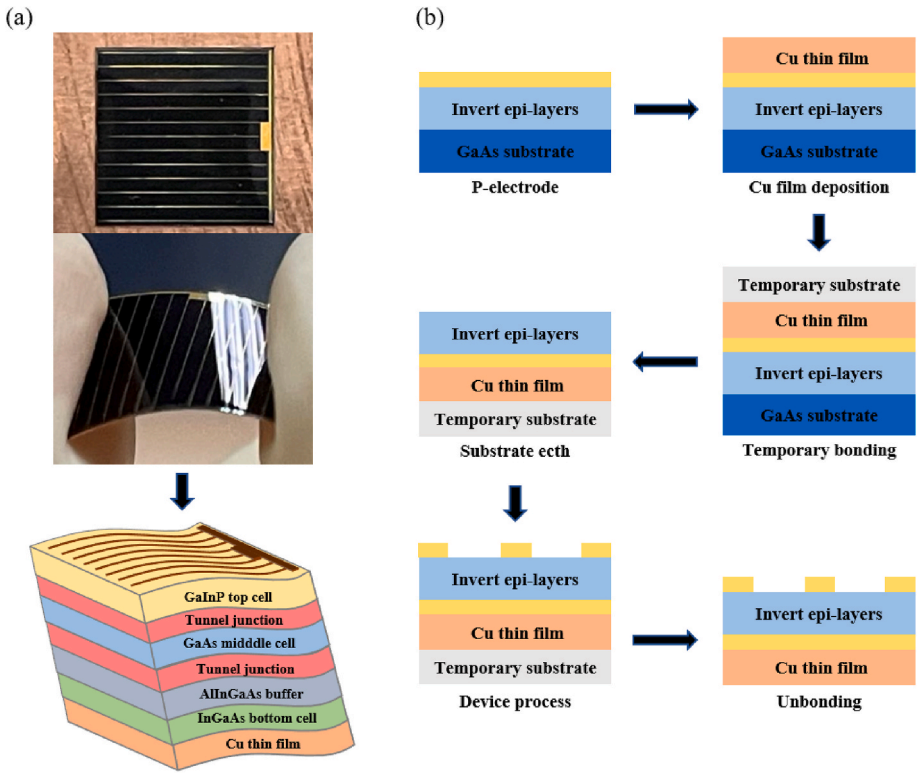

Fig. 1. (a) The photographs and schematic diagram of the stacked structure and (b) process flow diagram of the flexible GaInP/GaAs/InGaAs solar cells.

anti-aging performance of the solar cells without the protection of encapsulation materials is also crucial. However, there are few studies on the reliability of solar cells with unencapsulated flexible thin-film metal substrates under complex environmental stresses such as high temperature, high humidity and thermal cycling. With the development of the techniques such as inverted epitaxial growth [22–24], epitaxial lift-off (ELO) [25,26], and bonding between different homogeneous materials [27,28], the transfer of thin-film inverted epitaxial layer from a rigid substrate to a flexible substrate is realized, and the greater power-to-mass ratio is obtained [29]. The focus of our preliminary works is to simplify and optimize the fabrication art of flexible solar cells and to prepare devices with good performance. High-efficiency flexible triple-junction (3J) GaInP/GaAs/InGaAs solar cells have been fabricated by simple process steps such as electroplating metal thin-film flexible substrate, etching GaAs substrate, temporary bonding and so on [27,29]. Further accelerated aging tests are required to verify the process reliability and performance stability of flexible solar cells.

In this article, we investigated the optoelectronic performance attenuations of unencapsulated flexible 3J GaInP/GaAs/InGaAs solar cells under prolonged damp heat and thermal cycling tests. The solar cells were subjected to 85 °C/85% damp heat test for more than 1000 h and 420 cycles of thermal cycling test between −60 °C and 75 °C, respectively. The performance attenuations of flexible solar cells were less than 2% in both cases. The measurement results of external quantum efficiency (EQE) also confirmed the excellent optoelectronic properties of the solar cells. The slight decrease in open-circuit voltage was attributed to the increase in reverse saturation current due to the enhanced recombination, which was in good agreement with the calculation based on the two-diode model. The good performance of the unencapsulated flexible GaInP/GaAs/InGaAs solar cells in severe environments indicated the stable and reliable device fabrication art in the experiment.

2. Experimental

The inverted metamorphic (IMM) GaInP/GaAs/InGaAs solar cells were grown by metal-organic chemical vapor deposition (MOCVD). The lattice match subcells of GaInP and GaAs were deposited on GaAs substrate first, and then the lattice mismatched InGaAs bottom subcell was grown. The individual subcells were connected by thin tunnel junctions to allow the transport of the majority carriers dominated by tunneling mechanism [30,31]. The AlInGaAs buffer layer could effectively relieve the lattice mismatch stress. The specific stacking structure schematic is displayed in Fig. 1 (a). The inverted epitaxial layer required evaporating p-type electrode, depositing Cu film, bonding glass temporary substrate, etching the original GaAs substrate, and other fabrication processes to prepare effective flexible solar cell devices. The ARC structure of solar cells was TiO_x/Al_2O_3, which could effectively reduce the reflection of light. The simple process flow diagram is shown in Fig. 1 (b), and the detailed preparation methods are described in the research of Long et al. [27,32–34].

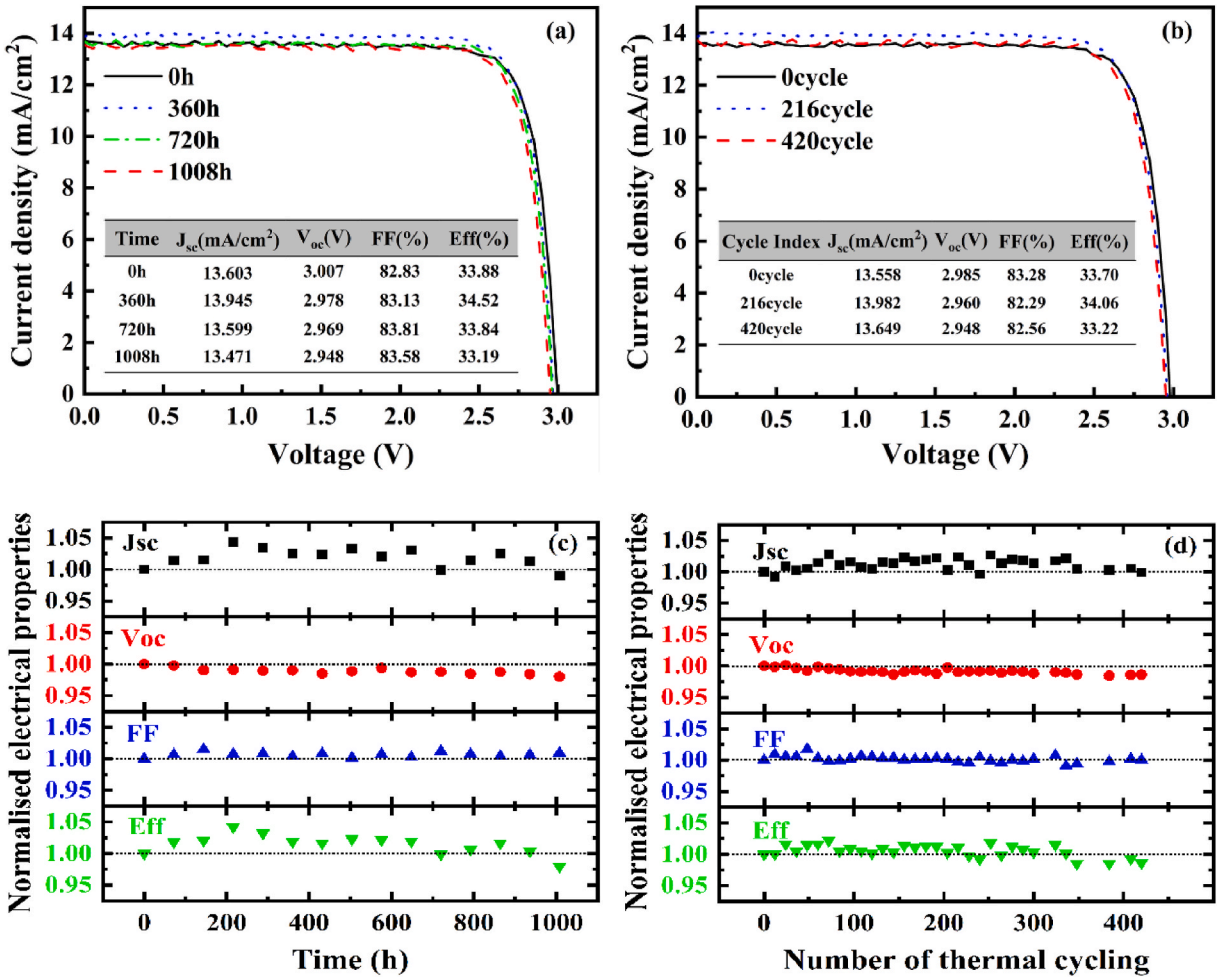

Fig. 2. *J-V* characteristic curves under the AM1.5G spectrum of the flexible GaInP/GaAs/InGaAs solar cell (a) after damp heat test at 85 °C and 85% RH for 0 h, 360 h, 720 h, 1008 h and (b) thermal cycling test between −60 °C and 75 °C after 0 cycle, 216 cycles, 420 cycles, the inserted tables are the absolute values of performance parameters; the normalized electrical properties of J_{sc}, V_{oc}, *FF*, and E_{ff} under long-term (c) damp heat test for 1008 h and (d) thermal cycling test after 420 cycles.

The solar cells in this paper are oriented to space stratospheric environment in practical applications. Accordingly, the successfully prepared 1 × 1 cm^2 flexible solar cells were exposed to high humidity and temperature (85% HR, 85 °C) and thermal cycling tests between −60 °C and 75 °C, respectively. In each reliability test, 5 solar cells were placed in the chamber with an air atmosphere. During aircrafts in the stratospheric environment, the low temperature at the bottom is around −55 °C (20 km), and the high temperature at the top can reach −3 °C–17 °C [35]. The solar cells will also absorb sunlight with higher temperature in actual operation, so the high temperature of the cycle is increased to 75 °C. On the other hand, water vapor exists at the bottom of the stratosphere due to its close proximity to the upper troposphere, and it has been demonstrated that there is a tendency for stratospheric water vapor to enhance [36]. The temperature from −60 °C to 75 °C is fully covered by the ambient temperatures experienced by airships in the stratospheric environment. In addition, we have to consider the storage of the solar cells on the ground, i.e., the solar cells will inevitably be exposed to high humidity environment. Both light and dark current-voltage (*I–V*) curves were measured on each cell every 72 h or 12 cycles under the solar simulator system in order to have a good tracking of the degradation, and the other electrical parameters of short-circuit current density (J_{sc}), open-circuit voltage (V_{oc}), fill factor (*FF*) and photoelectric conversion efficiency (E_{ff}) were also obtained. In order to avoid the effect of series resistance, the four-point probe method was used. The light source of the solar simulator is OSRAM 1000W short-arc xenon lamp, which can simulate the spectrum of AM1.5G standard irradiance. The specific *I–V* test methods could be seen in the research of Huang et al. [37]. The spectral responses of the cells were characterized using the EQE test, as detailed in the study of Long et al. [23,27,38].

3. Results and discussion

The performance of solar cells showed similar trends in aging tests, and we selected representative data for presentation. Fig. 2 (a)

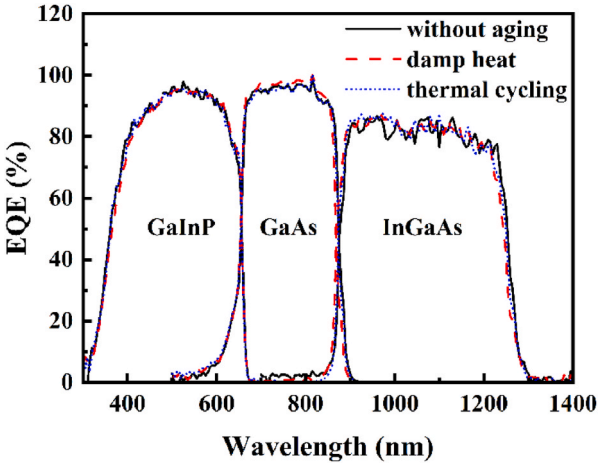

Fig. 3. The external quantum efficiency curves of flexible GaInP/GaAs/InGaAs solar cells without aging and after damp heat and thermal cycling tests.

Table 1
Short-circuit current density of each subcell of the solar cells without aging and after damp heat and thermal cycling tests.

Solar cells	$J_{sc\text{-}GaInP}$(mA/cm^2)	$J_{sc\text{-}GaAs}$(mA/cm^2)	$J_{sc\text{-}InGaAs}$(mA/cm^2)
Without aging	14.92	15.11	13.98
Damp heat	15.01	15.29	13.96
Thermal cycling	15.01	15.16	13.85

and (b) show the current density-voltage (*J-V*) characteristic curves of the flexible thin-film solar cells under the air mass 1.5G global (AM 1.5G) spectrum after damp heat test at 85 °C and 85% RH for 0 h, 360 h, 720 h, 1008 h and thermal cycling test between −60 °C and 75 °C after 0 cycle, 216 cycles, 420 cycles, respectively. The normalization changes of the performance parameters of the solar cells after damp heat test and thermal cycling test are shown in Fig. 2 (c) and (d), and some absolute values are given in the inserted tables in Fig. 2 (a) and (b). The efficiency of the solar cells is close to 34%, which is sufficient to demonstrate the stability of the performance under aging tests.

The performance attenuations of flexible solar cells were less than 2% in both cases, which were mainly manifested as the slow decline of V_{oc}. The *FF* and E_{ff} remained stable after aging tests which proved that the unencapsulated solar cells had a high resistance to heat and humidity and high durability to temperature changes. When the shunted subcell is the lowest photocurrent subcell in the 3J solar cell, an interesting fact of J_{sc} increase could be observed both in damp-heat and thermal cycling tests. In this case, the current-limiting subcell will be in a reverse-biased state at J_{sc} (multijunction solar cell at 0V), and increase its current generation when the shunt resistance becomes lower after aging [17,39]. However, the power of the solar cells barely decreased before and after the aging tests, which was in the first stage of its life cycle [12,40]. Longer period tests will be carried out to explore the specific lifetime of the solar cells in the future.

The external quantum efficiency (EQE) response of the solar cells can also demonstrated that the performance was not significantly degraded. As shown in Fig. 3, the EQE curves of the solar cells without aging and after damp heat and thermal cycling tests can be concluded that the excellent optoelectronic performance remained well after the aging tests. According to **Equation (1)**, the J_{sc} of each subcell could be calculated by the EQE (φ_{EQE}) and the spectral irradiance $(\varphi_{spec})_L$ [23],

$$J_{sc} = \frac{q\lambda}{hc}\int_0^{\infty} \varphi_{EQE}(\lambda) \bullet \varphi_{spec}(\lambda) d\lambda \# \tag{1}$$

where *h* is Planck's contant and *c* is the propagation speed of light in vacuum, *q* is the electron charge and λ is the wavelength. The calculated current density of each subcell is listed in Table 1. In the spectral response test of the subcells, because of the low shunt resistance of the InGaAs subcell, an appropriate bias voltage was added to the light bias [41].

The degradation of the flexible solar cells after damp heat and thermal cycling tests were mainly caused by the slight drop of V_{oc} (<2%). It's believed that under the aging environment, the lattice defects and surface defects were introduced into the material as the recombination centers, which accelerated the recombination inside the solar cells and thus reduced V_{oc}. Since the reverse saturation current in the dark *I–V* could effectively reflect the recombination process [42–44], we analyzed the behavior of the reverse saturation current under damp heat and thermal cycling tests.

Fig. 4 (a) and (b) shows the dark *I–V* curves of the solar cells after damp heat test at 85 °C and 85% RH for 0 h, 360 h, 720 h, 1008 h and thermal cycling test between −60 °C and 75 °C after 0 cycle, 216 cycles, 420 cycles, respectively. The dark *I–V* curve of the solar

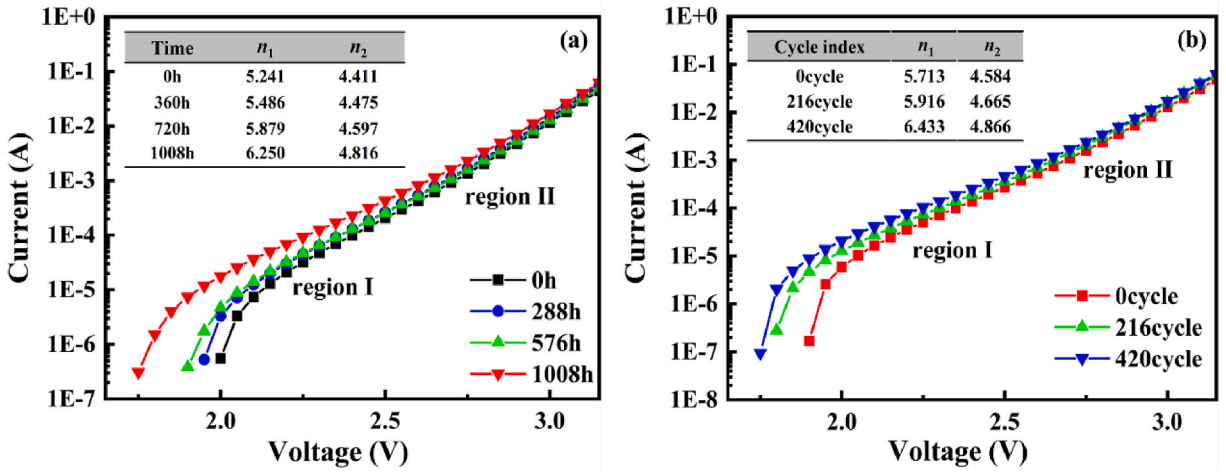

Fig. 4. Dark *I–V* curves of flexible GaInP/GaAs/InGaAs thin-film solar cells (a) after damp heat test at 85 °C and 85% RH for 0 h, 360 h, 720 h, 1008 h and (b) thermal cycling test between −60 °C and 75 °C after 0 cycle, 216 cycles, 420 cycles, the inserted tables are the calculated ideality factors n_1 and n_2.

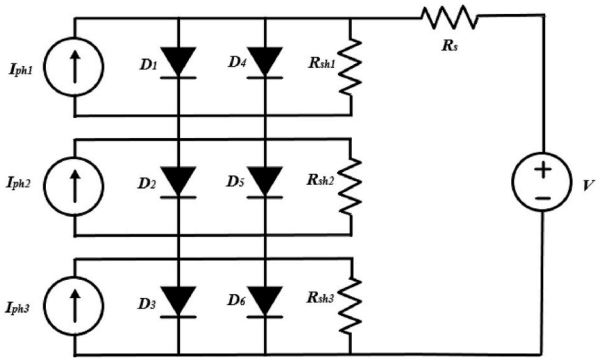

Fig. 5. Equivalent circuit diagram of a three-junction solar cell.

cell could be expressed as a double exponential function

$$I(V) = I_{rec}\left\{exp\left[\frac{q(V - IR_s)}{n_1 kT}\right] - 1\right\} + I_{dif}\left\{exp\left[\frac{q(V - IR_s)}{n_2 kT}\right] - 1\right\} + \frac{V - IR_s}{R_{sh}}\# \quad (2)$$

where I_{rec}, I_{dif} are the diode reverse saturation currents, n_1, n_2 are the ideality factors, q is the electron charge, k is Boltzmann's constant, T is the temperature, R_s and R_{sh} are the series and the shunt resistances. According to the equivalent circuit of the two-diode model, it can be divided into two regions representing different mechanisms. Region I is the recombination current I_{rec} and region II is the diffusion current I_{dif}, corresponding to the first two items of **Equation (2)**, respectively. The theoretically calculated ideality factors of single-junction solar cell come to $n_1 = 2$ considering the different recombination mechanisms and $n_2 = 1$ indicating the internal diffusion process of the solar cells at room temperature [45]. Since the 3J solar cell is made of three subcells connected in series, the n_1 and n_2 calculated by the dark *I–V* curves are not equal to 2 or 1. The result of the ideality factors is a combination of three subcells [46]. The numerical changes of the ideality factors for different times in damp heat and thermal cycling tests are given in the inserted tables in Fig. 4 (a) and (b). The total changes were $\Delta n_1 = 1.009$, $\Delta n_2 = 0.405$ for damp heat test, and $\Delta n_1 = 0.720$, $\Delta n_2 = 0.282$ for thermal cycling test. From the results, $\Delta n_1 > \Delta n_2$ illustrated that the increase of recombination current I_{rec} in the depletion region was more significant. The increased values of the ideality factors in both aging tests indicated that the corresponding shunt resistance affected by the recombination mechanism became much lower which was in consistent with the slow drop of V_{oc} in the light state. The recombination centers were introduced into the solar cells that the lifetime of the minority carriers was shortened and the reverse saturation current was increased during the progress of the aging tests.

In order to further understand the above situation, we calculated the *I–V* curves based on the two-diode model. The equivalent circuit of the 3J cell in Fig. 5 is an extension of the single-junction cell two-diode model [45]. The subcells of GaInP, GaAs and InGaAs are represented from top to bottom, respectively. In general, $I_{InGaAs} < I_{GaInP} < I_{GaAs}$. The *I–V* characteristics of the recombination and diffusion processes were analyzed by the two-diode model.

Table 2
The initial parameter values of the equivalent circuit model component.

Parameter	I_{ph}(mA)	I_{rec}(A)	I_{dif}(A)	n_1	n_2	R_{sh}(Ω)
GaInP	14.47	$2.09e^{-15}$	$4.3e^{-24}$	2	1	$1e^5$
GaAs	15.07	$3.45e^{-12}$	$1.2e^{-19}$	2	1	$1e^5$
InGaAs	13.63	$1.60e^{-8}$	$1.8e^{-16}$	2	1	$1e^5$

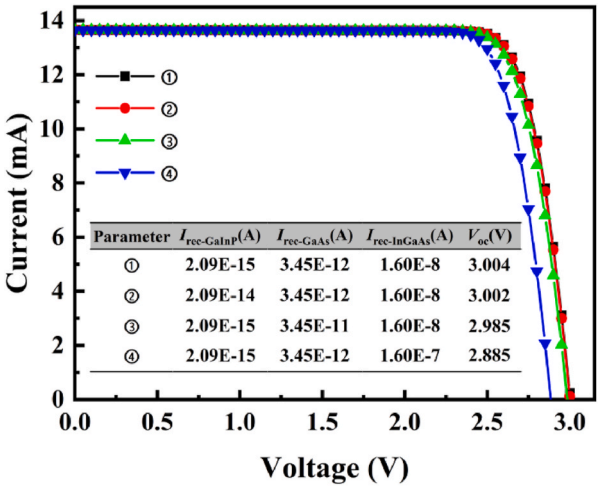

Fig. 6. The simulation results of the *I–V* curves, the inserted table are the I_{rec} of each subcell used in the simulation and the obtained V_{oc}.

The equivalent circuit diagram was simulated to evidence the explanation of the slight decrease in V_{oc} caused by the enhanced recombination. The sweep voltage range of the time varying power supply (V) is 0–3.5V, the series resistance $R_s = 9\Omega$, and the other component initial parameters such as the photogenerated current I_{ph}, the diode reverse saturation current I_{rec}, I_{dif}, the ideality factors n_1, n_2, and the shunt resistance R_{sh} of the subcell are given in Table 2. The initial magnitudes of the reverse saturation currents I_{rec} and I_{dif} in the simulation are approximately the same as the reverse saturation currents of each subcell given in the previous study [38]. The simulation result of the initial parameter values is shown as the curve ① in Fig. 6. In the simulation, V_{oc} was reduced by increasing the reverse saturation current I_{rec} of the subcells. The *I–V* curves ②, ③ and ④ in Fig. 6 show the simulation results after increasing the recombination current I_{rec} by one order of magnitude for the top, middle and bottom subcells, respectively. The inserted table in Fig. 6 shows the values of I_{rec} used by each subcell for *I–V* curves ①, ②, ③ and ④ and the values of V_{oc} obtained in the simulation. It was confirmed by simulation that the increase in the reverse saturation current I_{rec} of each subcell led to the decrease in V_{oc}. The decline trend of the simulated values about V_{oc} in Fig. 6 was similar to the results tested in the aging tests in Fig. 2 (a) and (b). When the reverse saturation current I_{rec} of each subcell increased by one order of magnitude respectively, it could be found that the lower the initial reverse saturation current of the subcell, the smaller the drop of V_{oc}.

4. Conclusions

In this paper, in order to evaluate the long-term stability of unencapsulated flexible GaInP/GaAs/InGaAs thin-film solar cells, we conducted damp heat and thermal cycling tests, respectively. The performance of the thin-film solar cells hardly decreased after the tests which indicated that the devices had damp resistance and thermal stress durability. The results of the EQE test also showed that the aging tests had no significant effect on the optoelectronic performance of solar cells. In the experiment, the substantial increase of the ideality factor associated with recombination mechanism demonstrated the introduction of more recombination centers during the aging tests, resulting in a slight decrease in V_{oc}. The above point of view was confirmed by the simulation results calculated by the diode model of multi-junction solar cells. The consequences of the experiences proved that the unencapsulated flexible solar cells had the ability to resist harsh environment, and the simple process flow of the flexible solar cells had distinguished reliability. In the near future, the stability of the encapsulated flexible solar cell can be further studied to verify the impact of the encapsulated process on the solar cells under the same severe conditions.

Author contribution statement

Xiaoxu Wu: performed the experiments, wrote the paper, analyzed and interpreted the data.
Junhua Long, Shulong Lu: conceived and designed the experiments.
Qiangjian Sun, Xia Wang, Zhitao Chen, Menglu Yu, Xiaolong Luo, Xuefei Li, Huyin Zhao: contributed reagents, materials, analysis

tools or data.

Data availability statement

Data will be made available on request.

Additional information

No additional information is available for this paper.

Declaration of competing interest

The authors declare that they have no known competing financial interests or personal relationships that could have appeared to influence the work reported in this paper.

Acknowledgements

This work is supported by the National Natural Science Foundation of China (Grant Nos. 61827823 and 62274176), the Natural Science Foundation of Jiangsu Province (Grant No. BK20220292), the Project of Science and Technology of Suzhou (No. SYC2022123), the program from SINANO (No. Y4JAQ21005), and the Jiangsu Funding Program for Excellent Postdoctoral Talent. Meanwhile, we are also grateful for the technical support from Nano-X, Nanofabrication Facility, and Platform for Characterization & Test of SINANO, CAS.

References

[1] M. Imaizumi, T. Takamoto, H. Sugimoto, T. Ohshima, S. Kawakita, Preliminary study on super radiation-resistant mechanical-stack triple-junction space solar cell: PHOENIX, in: IEEE 46th Photovoltaic Specialists Conference (PVSC), IEEE, 2019, pp. 1495–1498.
[2] S. Park, J.C. Bourgoin, H. Sim, C. Baur, V. Khorenko, O. Cavani, J. Bourcois, S. Picard, B. Boizot, Space degradation of 3J solar cells: I-Proton irradiation, Prog. Photovoltaics Res. Appl. 26 (2018) 778–788.
[3] J.M. Raya-Armenta, N. Bazmohammadi, J.C. Vasquez, J.M. Guerrero, A short review of radiation-induced degradation of III–V photovoltaic cells for space applications, Sol. Energy Mater. Sol. Cells 233 (2021), 111379.
[4] S. Kawakita, M. Imaizumi, K. Makita, J. Nishinaga, T. Sugaya, H. Shibata, S.I. Sato, T. Ohshima, High efficiency and radiation resistant InGaP/GaAs//CIGS stacked solar cells for space applications, in: 43rd IEEE Photovoltaic Specialists Conference (PVSC), IEEE, 2016, pp. 2574–2577.
[5] M.A. Green, E.D. Dunlop, J. Hohl-Ebinger, M. Yoshita, N. Kopidakis, K. Bothe, D. Hinken, M. Rauer, X. Hao, Solar cell efficiency tables (Version 60), Prog. Photovoltaics Res. Appl. 30 (2022) 687–701.
[6] T. Takamoto, T. Kodama, H. Yamaguchi, T. Agui, N. Takahashi, H. Washio, T. Hisamatsu, M. Kaneiwa, K. Okamoto, M. Imaizumi, K. Kibe, Paper-thin InGaP/GaAs solar cells, in: 4th World Conference on Photovoltaic Energy Conversion (WCPEC), IEEE, 2006, pp. 1769–1772.
[7] M. Imaizumi, T. Nakamura, T. Takamoto, T. Ohshima, M. Tajima, Radiation degradation characteristics of component subcells in inverted metamorphic triple-junction solar cells irradiated with electrons and protons, Prog. Photovoltaics Res. Appl. 25 (2017) 161–174.
[8] H.-F. Hong, T.-S. Huang, W.-Y. Uen, Y.-Y. Chen, Damp-heat induced performance degradation for InGaP/GaAs/Ge triple-junction solar cell, J. Nanomater. 2014 (2014) 1–6.
[9] S. Mekhilef, R. Saidur, M. Kamalisarvestani, Effect of dust, humidity and air velocity on efficiency of photovoltaic cells, Renew. Sustain. Energy Rev. 16 (2012) 2920–2925.
[10] I. Faye, A. Ndiaye, R. Gecke, U. Blieske, D. Kobor, M. Camara, Experimental study of observed defects in mini-modules based on crystalline silicone solar cell under damp heat and thermal cycle testing, Sol. Energy 191 (2019) 161–166.
[11] F. Khan, J.H. Kim, Performance degradation analysis of c-Si PV modules mounted on a concrete slab under hot-humid conditions using electroluminescence scanning technique for potential utilization in future solar roadways, Materials 12 (2019) 4047.
[12] M. Koehl, S. Hoffmann, S. Wiesmeier, Evaluation of damp-heat testing of photovoltaic modules, Prog. Photovoltaics Res. Appl. 25 (2017) 175–183.
[13] M. Kumar, A. Kumar, Performance assessment and degradation analysis of solar photovoltaic technologies: a review, Renew. Sustain. Energy Rev. 78 (2017) 554–587.
[14] Y. Tu, J. Wu, G. Xu, X. Yang, R. Cai, Q. Gong, R. Zhu, W. Huang, Perovskite solar cells for space applications: progress and challenges, Adv. Mater. 33 (2021), e2006545.
[15] S. van Riesen, A.W. Bett, Degradation study of III-V solar cells for concentrator applications, Prog. Photovoltaics Res. Appl. 13 (2005) 369–380.
[16] V. Orlando, M. Gabás, B. Galiana, P. Espinet-González, S. Palanco, N. Nuñez, M. Vázquez, K. Araki, C. Algora, Failure analysis on lattice matched GaInP/Ga(In)As/Ge commercial concentrator solar cells after temperature accelerated life tests, Prog. Photovoltaics Res. Appl. 25 (2017) 97–112.
[17] V. Orlando, I. Lombardero, M. Gabás, N. Nuñez, M. Vázquez, P. Espinet-González, J. Bautista, R. Romero, C. Algora, Temperature accelerated life test and failure analysis on upright metamorphic $Ga_{0.37}In_{0.63}P/Ga_{0.83}In_{0.17}As$/Ge triple junction solar cells, Prog. Photovoltaics Res. Appl. 28 (2019) 148–166.
[18] N. Nuñez, M. Vazquez, L. Barrutia, J. Bautista, I. Lombardero, J.C. Zamorano, M. Hinojosa, M. Gabas, C. Algora, Estimation of activation energy and reliability figures of space lattice-matched GaInP/Ga(In)As/Ge triple junction solar cells from Temperature Accelerated Life Tests, Sol. Energy Mater. Sol. Cells 230 (2021), 111211.
[19] P. Espinet-González, C. Algora, N. Núñez, V. Orlando, M. Vázquez, J. Bautista, K. Araki, Temperature accelerated life test on commercial concentrator III-V triple-junction solar cells and reliability analysis as a function of the operating temperature, Prog. Photovoltaics Res. Appl. 23 (2015) 559–569.
[20] K. Shimazaki, Y. Kobayashi, M. Takahashi, M. Imaizumi, M. Murashima, Y. Takahashi, H. Toyota, A. Kukita, T. Ohshima, S. Sato, et al., First flight demonstration of glass-type space solar sheet, in: 40th IEEE Photovoltaic Specialists Conference (PVSC), IEEE, 2014, pp. 2149–2154.
[21] T. Takamoto, H. Washio, H. Juso, Application of InGaP/GaAs/InGaAs triple junction solar cells to space use and concentrator photovoltaic, in: 40th IEEE Photovoltaic Specialists Conference (PVSC), IEEE, 2014, pp. 1–5.
[22] J.P. Samberg, C. Zachary Carlin, G.K. Bradshaw, P.C. Colter, J.L. Harmon, J.B. Allen, J.R. Hauser, S.M. Bedair, Effect of GaAs interfacial layer on the performance of high bandgap tunnel junctions for multijunction solar cells, Appl. Phys. Lett. 103 (2013), 103503.
[23] J. Long, D. Wu, X. Huang, S. Ye, X. Li, L. Ji, Q. Sun, M. Song, Z. Xing, S. Lu, Failure analysis of thin-film four-junction inverted metamorphic solar cells, Prog. Photovoltaics Res. Appl. 29 (2021) 181–187.
[24] J.F. Geisz, S. Kurtz, M.W. Wanlass, J.S. Ward, A. Duda, D.J. Friedman, J.M. Olson, W.E. McMahon, T.E. Moriarty, J.T. Kiehl, High-efficiency GaInP/GaAs/InGaAs triple-junction solar cells grown inverted with a metamorphic bottom junction, Appl. Phys. Lett. 91 (2007), 023502.

[25] S. Park, J. Simon, K.L. Schulte, A.J. Ptak, J.-S. Wi, D.L. Young, J. Oh, Germanium-on-Nothing for epitaxial liftoff of GaAs solar cells, Joule 3 (2019) 1782–1793.
[26] B. Gai, J.F. Geisz, D.J. Friedman, H. Chen, J. Yoon, Printed assemblies of microscale triple-junction inverted metamorphic GaInP/GaAs/InGaAs solar cells, Prog. Photovoltaics Res. Appl. 27 (2019) 520–527.
[27] J. Long, X. Li, Q. Sun, P. Dai, Y. Zhang, J. Xuan, F. Chen, M. Song, S. Honda, S. Uchida, S. Lu, Simple processing and analysis of flexible III–V multijunction solar cells using low-temperature transfer Technology, Sol. RRL 5 (2021), 2100066.
[28] D. Lackner, O. Höhn, R. Müller, P. Beutel, P. Schygulla, H. Hauser, F. Predan, G. Siefer, M. Schachtner, J. Schön, et al., Two-terminal direct wafer-bonded GaInP/AlGaAs//Si triple-junction solar cell with AM1.5g efficiency of 34.1, Sol. RRL 4 (2020), 2000210.
[29] J. Xuan, J. Long, Q. Sun, Y. Zhang, X. Li, X. Wang, Z. Chen, X. Wu, S. Lu, Flexible encapsulation and module of thin-film GaInP/GaAs/InGaAs solar cells, Sol. RRL 6 (2022), 2200371.
[30] M. Wanlass, P. Ahrenkiel, D. Albin, J. Carapella, A. Duda, K. Emery, D. Friedman, J. Geisz, K. Jones, A. Kibbler, et al., Monolithic, ultra-thin GaInP/GaAs/GaInAs tandem solar cells, in: 4th World Conference on Photovoltaic Energy Conversion (WCPEC), IEEE, 2006, pp. 729–732.
[31] G.J. Bauhuis, P. Mulder, J.J. Schermer, Ultra-thin, high performance tunnel junctions for III-V multijunction cells, Prog. Photovoltaics Res. Appl. 22 (2014) 656–660.
[32] Q. Sun, J. Long, X. Li, P. Dai, Y. Zhang, J. Xuan, X. Wang, Z. Chen, X. Wu, S. Lu, The diffusion effect of copper on the flexible GaInP/GaAs solar cells, IEEE Electron. Device Lett. 43 (2022) 584–587.
[33] J. Long, M. Xiao, X. Huang, Z. Xing, X. Li, P. Dai, M. Tan, Y. Wu, M. Song, S. Lu, High efficiency thin film GaInP/GaAs/InGaAs inverted metamorphic (IMM) solar cells based on electroplating process, J. Cryst. Growth 513 (2019) 38–42.
[34] Z. Chen, J. Long, Q. Sun, X. Wang, X. Wu, X. Li, M. Yu, X. Luo, H. Zhao, Y. Fu, S. Lu, Stress analysis of flexible GaInP/GaAs/InGaAs solar cells based on Cu thin-film substrates, Adv. Energy Sustain. Res. 4 (2022), 2200136.
[35] Y. Wang, X. Cao, T. He, F. Gao, D. Hua, M. Zhao, Observation and analysis of the temperature inversion layer by Raman lidar up to the lower stratosphere, Appl. Opt. 54 (2015) 10079–10088.
[36] A.E. Dessler, M.R. Schoeberl, T. Wang, S.M. Davis, K.H. Rosenlof, Stratospheric water vapor feedback, Proc. Natl. Acad. Sci. U.S.A. 110 (2013) 18087–18091.
[37] X. Huang, J. Long, D. Wu, S. Ye, X. Li, Q. Sun, Z. Xing, W. Yang, M. Song, Y. Guo, S. Lu, Flexible four-junction inverted metamorphic AlGaInP/AlGaAs/$In_{0.17}Ga_{0.83}As/In_{0.47}Ga_{0.53}As$ solar cell, Sol. Energy Mater. Sol. Cells 208 (2020), 110398.
[38] J. Long, Q. Sun, X. Li, P. Dai, M. Song, L. Zhu, H. Akiyama, J. Lu, S. Lu, Subcells analysis of thin-film four-junction solar cells using optoelectronic reciprocity relation, Sol. RRL 5 (2021), 2000542.
[39] I. Lombardero, C. Algora, Understanding the influence of shunts in the I–V curves and electroluminescence of multijunction solar cells, Sol. Energy Mater. Sol. Cells 204 (2020), 110236.
[40] N. Nunez, J.R. Gonzalez, M. Vazquez, C. Algora, P. Espinet, Evaluation of the reliability of high concentrator GaAs solar cells by means of temperature accelerated aging tests, Prog. Photovoltaics Res. Appl. 21 (2013) 1104–1113.
[41] F.T. Si, O. Isabella, M. Zeman, Artifact interpretation of spectral response measurements on two-terminal multijunction solar cells, Adv. Energy Mater. 7 (2016), 1601930.
[42] E.E. van Dyk, E.L. Meyer, Analysis of the effect of parasitic resistances on the performance of photovoltaic modules, Renew. Energy 29 (2004) 333–344.
[43] P. Dai, L. Ji, M. Tan, S. Uchida, Y. Wu, A. Abuduwayiti, M. Heini, Q. Guo, L. Bian, S. Lu, H. Yang, Electron irradiation study of room-temperature wafer-bonded four-junction solar cell grown by MBE, Sol. Energy Mater. Sol. Cells 171 (2017) 118–122.
[44] L. Ji, M. Tan, C. Ding, K. Honda, R. Harasawa, Y. Yasue, Y. Wu, P. Dai, A. Tackeuchi, L. Bian, et al., The striking influence of rapid thermal annealing on InGaAsP grown by MBE: material and photovoltaic device, J. Cryst. Growth 458 (2017) 110–114.
[45] R. Hussein, D. Borchert, G. Grabosch, W.R. Fahrner, Dark I-V-T measurements and characteristics of (n) a-Si/(p) c-Si heterojunction solar cells, Sol. Energy Mater. Sol. Cells 69 (2001) 123–129.
[46] A. Braun, N. Szabó, K. Schwarzburg, T. Hannappel, E.A. Katz, J.M. Gordon, Current-limiting behavior in multijunction solar cells, Appl. Phys. Lett. 98 (2011), 223506.